Förster resonant energy transfer from an inorganic quantum well to a molecular material: Unexplored aspects, losses, and implications to applications

ARTICLE *in* THE JOURNAL OF CHEMICAL PHYSICS · DECEMBER 2015

Impact Factor: 2.95 · DOI: 10.1063/1.4935963

4 AUTHORS, INCLUDING:

G. Itskos

University of Cyprus

51 PUBLICATIONS **1,225** CITATIONS

SEE PROFILE

Stelios A Choulis

Cyprus University of Technology

98 PUBLICATIONS **5,469** CITATIONS

SEE PROFILE

AIP | The Journal of Chemical Physics

Förster resonant energy transfer from an inorganic quantum well to a molecular material: Unexplored aspects, losses, and implications to applications

G. Itskos, A. Othonos, S. A. Choulis, and E. Iliopoulos

Citation: The Journal of Chemical Physics **143**, 214701 (2015); doi: 10.1063/1.4935963
View online: http://dx.doi.org/10.1063/1.4935963
View Table of Contents: http://scitation.aip.org/content/aip/journal/jcp/143/21?ver=pdfcov
Published by the AIP Publishing

Förster resonant energy transfer from an inorganic quantum well to a molecular material: Unexplored aspects, losses, and implications to applications

G. Itskos,[1,a)] A. Othonos,[2] S. A. Choulis,[3] and E. Iliopoulos[4]
[1]*Experimental Condensed Matter Physics Laboratory, Department of Physics, University of Cyprus, Nicosia 1678, Cyprus*
[2]*Laboratory of Ultrafast Science, Department of Physics, University of Cyprus, Nicosia 1678, Cyprus*
[3]*Molecular Electronics and Photonics Research Unit, Department of Mechanical Engineering and Materials Science and Engineering, Cyprus University of Technology, Limassol 3603, Cyprus*
[4]*Microelectronics Research Group, IESL, FORTH and Physics Department, University of Crete, P.O. Box 1385, 71110 Heraklion-Crete, Greece*

(Received 12 August 2015; accepted 27 October 2015; published online 1 December 2015)

A systematic investigation of Förster resonant energy transfer (FRET) is reported within a hybrid prototype structure based on nitride single quantum well (SQW) donors and light emitting polymer acceptors. Self-consistent Schrödinger-Poisson modeling and steady-state and time-resolved photoluminescence experiments were initially employed to investigate the influence of a wide structural parameter space on the emission quantum yield of the nitride component. The optimized SQW heterostructures were processed into hybrid structures with spin-casted overlayers of polyfluorenes. The influence of important unexplored aspects of the inorganic heterostructure such as SQW confinement, content, and doping on the dipole-dipole coupling was probed. Competing mechanisms to the FRET process associated with interfacial recombination and charge transfer have been studied and their implications to device applications exploiting FRET across heterointerfaces have been discussed. © *2015 AIP Publishing LLC.* [http://dx.doi.org/10.1063/1.4935963]

I. INTRODUCTION

The integration of solution-processed with epitaxial semiconductors opens up the possibility for heterogeneous structures with novel functionalities and properties. Electronic communication in such assemblies typically relies on charge transfer across the heterointerface(s), being susceptible to interfacial recombination. Resonant electronic interactions that promote energy instead of charge transfer can provide an alternative contactless pathway that circumvents some of the losses associated with charge recombination and transport.

Pioneering theoretical work has demonstrated the feasibility of such an approach in the so-called weak coupling regime, in a prototype planar structure that supports Forster resonant energy transfer (FRET)[1,2] from an inorganic single quantum well (SQW) to a light emitting organic medium.[3–5] Experimental verification of the proposal came some years later using (Ga,In)N SQWs as energy donors and close-packed monolayers of CdSe/ZnS core/shell nanocrystals as energy acceptors, demonstrating high FRET efficiencies reaching 55% at room temperature.[6] Soon after, efficient FRET was observed for the first time in an inorganic-organic material hybrid combining (Ga,In)N SQWs and light emitting polyfluorenes.[7] The universality of the FRET excitation across heterogeneous planar interfaces was demonstrated with a series of experiments on photo-pumped structures, which include among others, combinations of ZnO QWs with various organic oligomers,[8,9] ZnO nanoparticles with conjugated polymers,[10] J-aggregates with nanocrystals,[11] GaAs QWs with organic dyes,[12] nitride SQWs with metallic nanoclusters,[13] and CdSe nanostructures with graphene layers.[14,15]

The proof-of-principle in an electrical-biased device was early demonstrated in a hybrid LED comprising a n-i-p InGaN QW structure with CdSe nanocrystals, producing color-conversion efficiencies of 13%.[16] Furthermore, the potential for white light generation mediated by FRET was highlighted based on combinations of (Ga,In)N QW donors and blends of polyfluorenes[17,18] or CdSe/ZnS core/shell nanocrystals.[19,20] In addition, the inverse process of FRET from organic to inorganic materials as a light harvesting paradigm proposed by Dexter[21] was treated theoretically[22,23] and experimentally demonstrated in hybrids composed of colloidal nanocrystals and GaAs p-i-n structures[24] and J-aggregates with nanocrystal monolayers.[11] Demonstration of FRET in appropriately engineered or patterned nanostructures, allowed the increase of the hetero-interfacial area, attesting to the suitability of the FRET excitation in practical light emitting and light harvesting devices.[11,16,24–26]

Further studies have probed important aspects of the resonant energy transfer process that include the dependence on donor-acceptor distance and dimensionality [theory[3–5,27,28] and experiment[8,9,29]], the temperature variation and correlation with the dominant at each temperature photoexcitation species, i.e., free/bound excitons or unbound electron-hole pairs [theory[4,5,27,30,31] and experiment[7,10,29,32,33]], the impact of the relative orientation of donor-acceptor dipoles [theory[34]] and the influence of interface quality, surface characteristics, and hybrid bonding.[8,9,29] Further details on theoretical and

a)E-mail: itskos@ucy.ac.cy

experimental aspects of the topic can be obtained in the authoritative review of Ref. 27 and references within.

Despite the knowledge accumulated recently on the topic, there exist important material and structural parameters affecting the FRET across such heterogeneous interfaces that remain weekly explored or completely unexplored. Their investigation is important both in terms of fundamental science as well as in order to optimize the efficiency and access the potential of FRET-based excitation schemes in practical devices. The exact influence of the donor emission quantum yield (QY), quantum confinement, and structural characteristics of the inorganic structure on the energy transfer process have not been systematically studied. Furthermore, it appears that there is more room on studies that probe the losses mediated by the hybrid interface that compete with the FRET process, reducing its overall efficiency. Finally, it has not been thus far explicitly examined whether and how electronic doping affects the energy transfer process. This is a crucial investigation that can attest to the applicability of FRET in commercial electrical-excited p-i-n structures.

It appears appropriate that the influence of such parameters on FRET should be probed in a well-studied, easily reproducible hybrid architecture such as the one originally proposed,[3,4] i.e., a near-surface inorganic SQW on a nanoscale proximity to an organic absorber film. This is a simple architecture, used to demonstrate efficient FRET with various combinations of QW-thin film materials, and allows the preparation of well-defined planar hybrid interfaces. (Ga,In)N QWs and light emitting polymers (LEPs) have separately been the focus of intense research and recently being combined in novel hybrid light emitting devices.[17,35,36] They appear naturally as a promising donor-acceptor energy pair for the aforementioned studies. Despite the high dislocation densities, (Ga,In)N quantum wells exhibit high emission yield at room temperature. Importantly, due to the relatively weak nitride surface recombination,[37] nitride QWs appear to retain much of their luminescent efficiency when placed at close proximity to the surface,[38–40] a prerequisite for strong donor-acceptor FRET coupling.[1,2] The availability of excellent polymer absorbers from the polyfluorene family in the emission region of such QWs ensures good overlap of donor (QW) emission and acceptor (polymer) absorption, as required for efficient dipole-dipole coupling.[1] Importantly, efficient FRET in such material combinations has been repeatedly demonstrated[7,17,18,26,29] and hybrid characteristics such as the nitride/polyfuorene interface and energy band alignment have been recently investigated.[41]

II. EXPERIMENTAL

We report here systematic studies of FRET in hybrid structures of (Ga,In)N SQWs placed in nanometer-scale proximity to ultrathin films of polyfluorenes. The SQW heterostructures were grown by radio frequency plasma assisted molecular beam epitaxy (RF-MBE) on (0001) GaN/c-Al_2O_3 templates. A 0.5 μm GaN buffer layer was employed in all cases. The SQWs were grown at a growth temperature range of 590 °C–650 °C, under slightly III-rich growth conditions, with nominal InN mole fractions spanning in the range of 0.06–0.15, and thicknesses in the range of 2–3.5 nm. The SQWs were subsequently capped with a top GaN or (Al,Ga)N cap of 4–10 nm thickness, grown at 705 °C or at the same growth temperature as that used for the QW material to avoid growth interruption. To study the effect of electronic doping, a fraction of SQWs were capped with barriers doped with Si up to the level of 2×10^{18} cm^{-3}. The hybrid structure was completed by deposition of the polyfluorene homopolymer poly(9,9-dioctyfluorenyl-2,7-diyl) end-capped with N,N-bis (4-methylphenyl)-aniline, typically known as PFO or the polyfluorene copolymer poly[(9,9-dioctyl-2,7-divinylenefluorenylene)-alt-co-(9,10-anthracene)]. The hybrid structure schematic and the polymers chemical formulas are displayed in Figure 1. The materials were purchased from American Dye Source, Inc., and will be referred to as PF1 and PF2, respectively, in the manuscript. Powder from the materials was dissolved in chlorobenzene at concentrations of 1-2 mg/ml. The solutions were stirred at 80-85 °C for more than 1 h and spin-coated on top of the QW wafers that have been cleaned by acetone and isopropyl alcohol. Reference polymer films were also deposited on c-plane GaN and sapphire substrates. Spin-casting speeds of ~4500–5000 rpm were used, followed by a 6000 rpm drying step, producing thin uniform films in the 10-20 nm range.

Steady-state photoluminescence (PL), photoluminescence excitation (PLE), and time-resolved PL (TR-PL) experiments were performed in a Fluorolog 3 Horiba Jobin

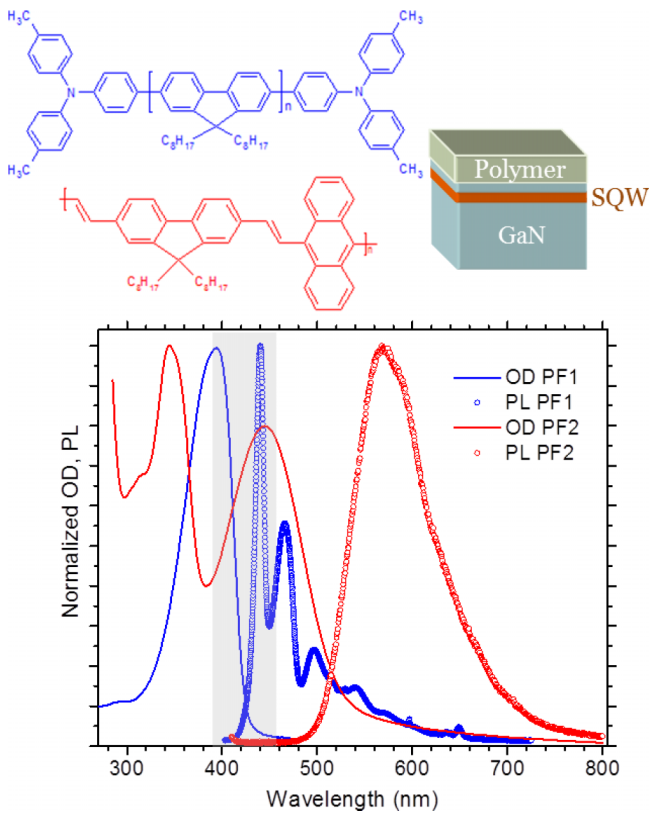

FIG. 1. Normalized absorbance (solid) and PL (scatter) excited at 350 nm of ~10 nm thick films of the polyfluorenes PF1 (blue) and PF2 (red), employed to complete the hybrid structures. The grey highlighted area indicates the PL spectral range of the inorganic (Ga,In)N SQWs hybrid component.

Yvon spectrometer, based on an iHR320 monochromator equipped with a visible photomultiplier tube (Horiba TBX-04 module). Steady-state PL was excited either non-resonantly at 350 nm using the monochromatically filtered output (double monochromator) of an Ozone-free 450 W Xenon Arc lamp or quasi-resonantly at 375 nm using the output beam of a 7 mW Oxxius laser diode. PLE excitation was produced by the same combination of the double monochromator with the xenon lamp, monitoring the respective PL peak within a 5 nm spectral window. Time-resolved PL was measured using a time correlated single photon counting (TCSPC) method in combination with the visible PMT employed in the steady-state measurements. The PL was excited by a NanoLED laser diode at 375 nm (N-375L) operating at 100 KHz with a pulse FWHM of ~100 ps. The system exhibits a time resolution of ~50 ps after reconvolution with the instrument response function using the DAS6 (Horiba Jobin Yvon) software analysis package. The decays were recorded at the respective PL peak within a spectral window of 5-10 nm. PL spectra were corrected to account for the spectral response of the grating and the PMT used. All PL data have been acquired with samples placed in vacuum (~10^{-3} mbar) in a Janis VPF liquid nitrogen optical cryostat within the 77-300 K temperature range.

III. DATA AND DISCUSSION

A. Optimization of the nitride quantum wells

Normalized absorbance (optical density) of PF1 and PF2 films on sapphire and PL spectra from identical films on a surface (Ga,In)N/GaN SQW are displayed on Figure 1. PF1 exhibits singly peaked absorption at ~396 nm and characteristic PL vibronics, with a 0-0 peak at ~440 nm. PF2 contains two absorption bands at ~345 nm and ~445 nm and a red-shifted featureless PL, peaked at 570 nm. The graph's greyish highlighted area indicates the PL spectral range of the nitride SQWs grown, confirming the good spectral overlap of their emission with the PF1 and/or PF2 absorption required for efficient hybrid dipole-dipole coupling.

According to the original model by Förster,[1] the FRET rate k_{FRET} is dependent on experimentally observed quantities of the interacting donor-acceptor dipoles,

$$k_{FRET} \sim \frac{\kappa^2 \varphi_D \Omega}{\tau_D n^4 R^6}, \tag{1}$$

where κ is the dipole-dipole orientation factor, φ_D and τ_D are the fluorescence quantum yield and the radiative lifetime of the donor, respectively, Ω is the spectral overlap of the acceptor molar absorptivity $\alpha_A(\lambda)$ with the area-normalized emission spectra of the donor, n the refractive index of the intervening medium, and R is the center to center dipole separation.

Even though the model does not exactly apply to the plane-to-plane dipole interaction of our case,[29] FRET is expected to keep dependencies with the quantities of (1). It appears that two out of those quantities, i.e., φ_D and τ_D are intrinsic properties of the SQW structure in the absence of the hybrid interaction. Based on this, our study focused initially on the influence of various intrinsic SQW structural parameters on the parameters φ_D and τ_D. The expected benefits of the optimization process would be (i) to produce surface InGaN SQWs with high radiative efficiency at room temperature and (ii) to simultaneously enhance the FRET efficiency in hybrid structures of such quantum wells with polyfluorene thin overlayers.

The study appears a necessity as apart from few recent reports,[38–40,42] the competition of radiative versus surface recombination in such near-surface nitride SQWs remains underexplored. The study involved the systematical investigation of the influence of the following key QW growth parameters: (1) SQW width, (2) SQW InN mole fraction, (3) SQW growth temperature, (4) top cap thickness, (5) top cap content, (6) top cap growth temperature, and (7) top cap n-doping.

Self-consistent Schrödinger-Poisson (SCSP) modeling was initially employed to explore the aforementioned SQW heterostructure design parameters space. The numerical model involved the solution of 1-D coupled Schrödinger-Poisson equations of the form

$$-\frac{\hbar^2}{2}\left(\frac{\partial}{\partial z}\left(\frac{1}{m^*}\frac{\partial}{\partial z}\right) - q_e \cdot \varphi(z) + \Delta E_C(z)\right)\Psi_k(z) = E_k \Psi_k(z), \tag{2}$$

$$\frac{\partial}{\partial z}\left(\varepsilon \cdot \frac{\partial}{\partial z}\varphi(z) - P_{SP}(z) - P_{PZ}(z)\right) = q_e \cdot \left(n[\varphi] - N_D^+[\varphi]\right), \tag{3}$$

where $\varphi(z)$ and $\Delta E_c(z)$ are the electrostatic and the heterostructure potential and $P_{SP}(z)$ and $P_{PZ}(z)$ the spontaneous and piezoelectric polarization field, respectively. The piezoelectric polarization field is deduced assuming all layers coherently, biaxially, strained to the underlying GaN substrate,

$$P_{PZ}(z) = 2 \cdot \frac{a - a_0}{a_0} \cdot \left(e_{11} - e_{33} \cdot \frac{c_{13}}{c_{33}}\right), \tag{4}$$

where a the in-plane lattice constant of the strained layer, a_0 the corresponding in-plane lattice constant in the case of unstrained conditions, and c_{13}, c_{33}, and e_{13}, e_{33} are the elastic and piezoelectric constants, respectively. All relevant parameters used were those of Ambacher *et al.*[43] In the case of Poisson equation, only the electron density $n[\varphi]$ and the ionized donor density $N_D^+[\varphi]$ are considered, since no acceptors were taken into account and the occupation probability of hole states is negligible in those structures. The electron density is obtained as the sum of all electron bound states,

$$n[\varphi] = \sum_{k=1}^{m} |\Psi_k(z)|^2 \cdot \int_{E_k}^{\infty} \frac{dE}{1 + \exp\left(\frac{E - E_F}{kT}\right)} \tag{5}$$

and the ionized donor density is given, assuming a donor degeneracy factor of 2, by

$$N_D^+[\varphi] = \frac{N_D(z)}{1 + 2 \cdot \exp\left(\frac{E_F - E_D}{kT}\right)}, \tag{6}$$

where, in the above, E_F the Fermi energy level, E_D the donor level, and N_D the considered donor concentration.

The model assumed n-type GaN(0001) substrates, with carrier density of 5×10^{16} cm^{-3} and thickness of 1 μm. The equilibrium Fermi level was considered pinned by the (Al)GaN surface states. For the case of GaN, this was 0.7 eV below the conduction band edge. Based on the extracted electron and holes eigenstates and eigenenergies, the expected QW optical transition energy and the QW confined electron-hole eigenstates overlap integral, were calculated. In Figure 2, an example of the calculated heterostructure profile in the near surface region and the relevant electon-hole eigenfunction is presented for the case of a $In_{0.07}Ga_{0.93}N$ 2.5 nm QW with 5 nm undoped ($n_d = 5 \times 10^{16}$ cm^{-3}) GaN barrier. The calculation clearly indicates that the electron wavefunction strongly penetrates the top GaN barrier resulting in a rather weak SQW confinement. Furthermore, the electron-hole eigenfunction appear partly separated, due to the polarization field, resulting in a reduced wavefunction overlap and thus a reduced SQW optical transition oscillator strength.

The calculations also probed the influence of QW composition and thickness on the energy of the optical transition and its strength, as defined by the electron-hole wavefunction overlap integral. In Figure 3, the corresponding contour maps for QW InN mole fraction in the range of 0.05–0.15 and QW thickness in the range of 1.5–5.0 nm are shown. In all cases, an undoped 5.0 nm GaN barrier was considered. As expected, the SQW optical transition energy is strongly dependent on both SQW thickness and composition as observed in Figure 3(a). The electron-hole overlap integral appears to strongly decrease as the QW becomes wider, while it appears to have a weaker dependence on the QW composition, as observed in Figure 3(b).

To reduce the electron wavefunction leakage into the top GaN barrier, the SCSP calculations examined the case of an asymmetric well, produced via Al incorporation in the top cap layer. In Figure 4(a), the results of the modelling for the case of a 5 nm thick (Ga,Al)N barrier with a relatively low AlN

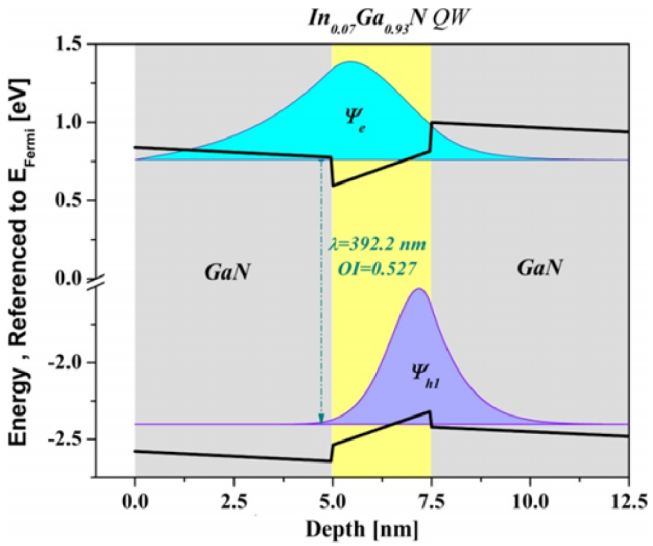

FIG. 2. The output of SCSP calculations displaying the heterostructure profile and the QW electron-hole eigenfunctions for QW InN mole fraction equal to 0.07 and thickness of 2.5 nm. The barrier is an undoped 5 nm GaN layer.

mole fraction of 0.08 are shown. The calculation shows that the introduction of Al indeed results in a better confinement of the electron wavefuction, producing an increase of the overlap integral by 20% and a small blue-shift of the SQW optical transition by ~3 nm compared to the symmetric SQW structure of Figure 2. However, a further increase of the barrier AlN mole fraction to 0.15 results in the appearance of hole states within the (Ga,Al)N barrier, as shown in Figure 4(b). The confined hole state energy appears ~38 meV lower that the quantum well hole states, making the former the ground state of holes in the heterostructure.

To validate the results of the modelling, we performed a sequence of RF-MBE growth runs where the relevant characteristics of the SQWs were systematically varied and probed by photoluminescence spectroscopy. Figure 5 displays characteristic spectra probing the effect of the well width, top cap content, and growth temperature on the room temperature SQW emission. All other growth parameters were kept fixed to the following values: InN mole fraction of ~0.07, SQW growth temperature of 600 °C, and top GaN cap thickness of ~4 nm. Figure 5(a) contains the results of steady-state comparative PL spectra from three QWs with different well width. The emission spectra are attributed to radiative recombination from confined electron and hole states in the SQWs. The superimposed fringes are the result of optical interference produced within the ~10 nm thick GaN structure as emitted QW light interferes with light reflected at the GaN/c-Al_2O_3 interface due to the index of refraction mismatch of c-Al_2O_3 of ~1.78 and GaN of ~2.45 eV at the spectral range of the QW emission.[44] The figure indicates a systematic photoluminescence quenching along with a red-shift of the PL peak position as the well width increases in agreement with the SCSP results of Figure 3(a). The quenching implies a reduction of φ_D with SQW well width; similar trends are obtained at lower sample temperatures down to 77 K. Figure 5(b) contains the time-resolved PL data from the same samples. An adequate approximation of the decays can be obtained using a bi-exponential fit with a short dominant time constant of τ_1 = 0.3-0.4 ns and a weaker, longer component of τ_2 = 2.0-2.5 ns. The SQW PL lifetime is obtained by adding the two decay constants weighted by their relative contribution. Increase of the well width appears to increase the relative contribution of τ_1 at the expense of τ_2, resulting in SQW lifetime shortening.

Figure 5(c) contains comparative spectra of four SQWs, two of them terminated by GaN top caps grown at different temperatures, i.e., 600 °C and 705 °C and the other two terminated by an (Al,Ga)N barrier grown at 705 °C with relative low (0.1) and high (0.3) AlN mole fraction. Lowering of the cap growth temperature appears beneficial to the PL intensity. For the same cap growth temperature (705 °C), an increase in the confinement by incorporation of 10% Al in the top barrier appears to also improve the PL. Further increase of the Al content results in an almost complete quenching of the QW PL. The results are in close agreement with the calculation findings of Figure 4. The increase of the luminescence for low Al content SQWs is attributed to the beneficial effect of confinement on the QW electron-hole wavefunction overlap. Larger Al incorporation results in hole localization at the

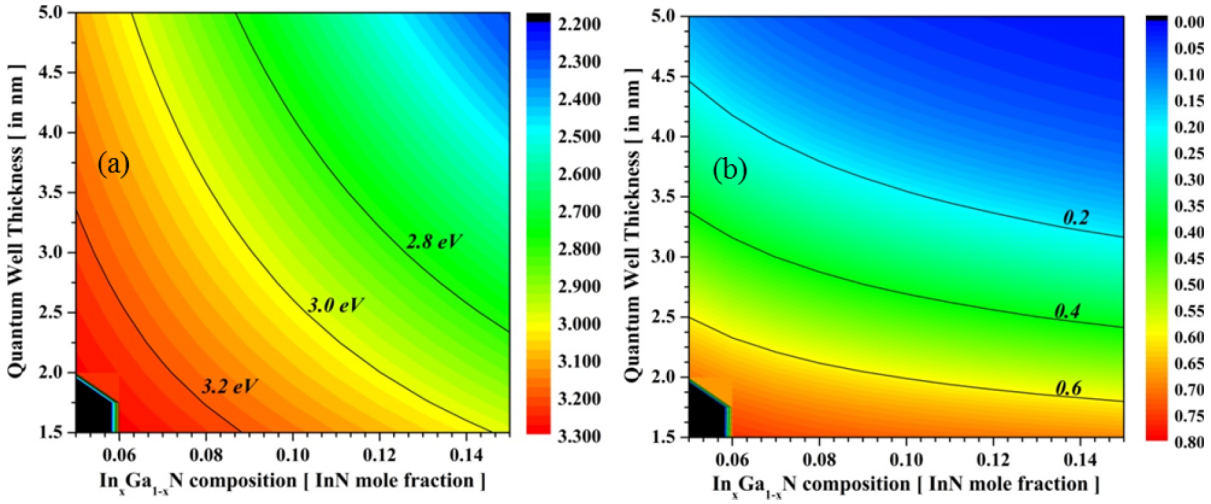

FIG. 3. Contour maps produced by the SCSP modeling, showing the effect of SQW composition and thickness on (a) the energy and (b) oscillator strength of the QW optical transition.

barrier and quenching of the PL emission as a result of the proximity of the hole states to the structure surface.

B. Characteristics of FRET in the hybrid structures

To investigate the FRET characteristics in our samples, an experimental protocol was introduced based on steady-state and time-resolved PL and PLE experiments. The routine was performed in each hybrid structure produced and comprises the three separate experiments, displayed in Figure 6. The displayed data are typical of hybrid structures based on PL-optimized SQWs, employing a surface (Ga,In)N/GaN SQW with a 2 nm QW width and top GaN cap of 4 nm followed by an overlayer of ~10 nm from the homopolymer PF1. On Figure 6(a), the PLE spectra of a reference PF1 film on sapphire (blue) are contrasted with the PLE from the PF1 film on the SQW wafer (red). The former exhibits a qualitatively similar spectral shape to the polymer absorbance (see Figure 1); on the contrary, the PLE spectrum from the QW deposited polymer film contains a new, distinct peak at ~402 nm. The peak appears to coincide spectrally with the peak of the QW PL spectrum (green area), indicating the QW as the origin of the peak. We can thus conclude that in addition to direct laser excitation, the polymer emission contains a contribution due to QW pumping. Previous work has demonstrated that the radiative contribution of this pumping process, for a planar hybrid structure with a very thin polymer overlayer such as the one employed in our studies, is relatively small.[29] To conclusively confirm and access the predominantly non-radiative character of the energy transfer process, time-resolved PL experiments were employed.

Figure 6(b) displays the results of such an experiment, probing the PL decay of the QW energy donor in the absence (blue) and presence (red) of the PF1 overlayer. The QW decay in the presence of the polymer contains a fast exponential term and a non-exponential tail at longer times that contributes weakly on the average lifetime. For the sake of simplicity, bi-exponential fits used for the pristine QW transients are also employed to describe the hybrid decay. The fitting produces average lifetimes of $\tau_{bare} \sim 0.74$ ns and $\tau_{hybrid} \sim 0.38$ ns

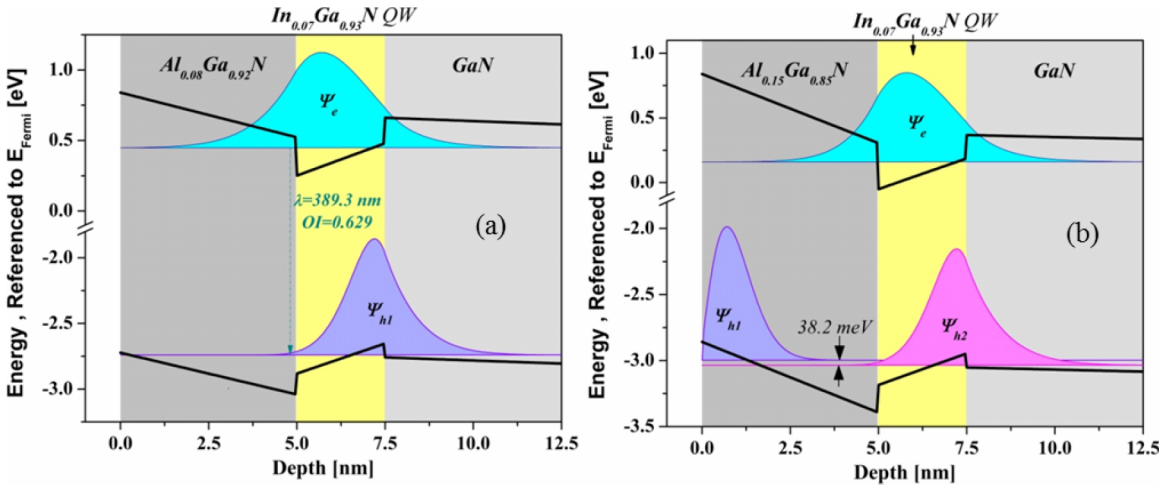

FIG. 4. Heterostructure profile and energy states for (a) a SQW with a 5 nm AlGaN top cap with an AlN mole fraction of 0.08, (b) a SQW with the same characteristics with a top barrier with AlN mole fraction of 0.15.

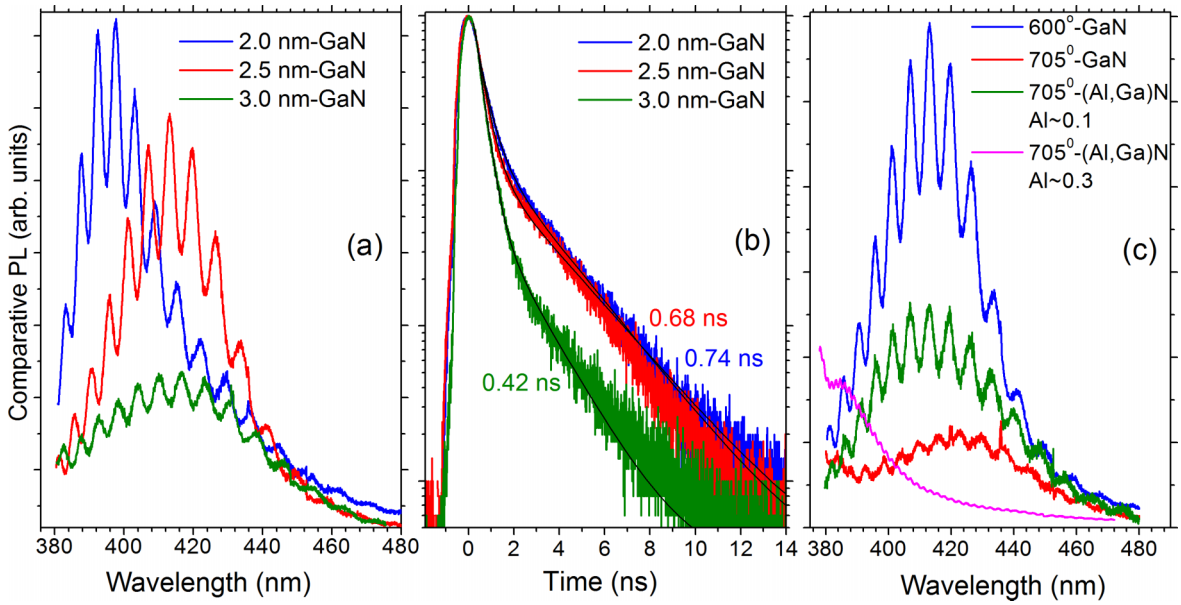

FIG. 5. (a) Comparative 300 K PL, excited at 350 nm, from (Ga,In)N SQWs with different well widths. The legend refers to the SQW well width. (b) Time-resolved PL decays of the same SQWs monitoring the QW peak within a 10 nm spectral window, along with bi-exponential curve fits (black lines). The average PL lifetime obtained by the fitting is displayed in the proper color-coding for each QW. (c) Comparative PL spectra, non-resonanlty excited at 350 nm, from surface SQWs with different top cap contents, GaN or (Al,Ga)N and different top cap growth temperatures.

for the QW in the absence and presence of the PF1 layer, respectively. The quenching of the QW lifetime in the hybrid structure typically signifies the presence of FRET across the heterointerface. Using the equation for the FRET efficiency Φ_{FRET},[29]

$$\Phi_{FRET} = \frac{\tau_{hybrid}^{-1} - \tau_{bare}^{-1}}{\tau_{hybrid}^{-1}} \cdot 100\% \approx 49\%. \quad (7)$$

The simple analysis assumes that the QW lifetime quenching in the hybrid structure is exclusively due to the FRET process to the polymer exciton states, so values obtained with this methodology represent an upper bound value for the FRET efficiency. Figure 6(c) contains the fluorescence decay of the polymer, i.e., acceptor of energy, by spectrally and temporarily monitoring the 0-0 vibronic of PF1 films deposited on the QW wafer (red) and a reference GaN substrate (blue). The former decays exhibit significantly slower signal rise time and a larger lifetime compared to the latter. Apart from a small contribution from a long-decay channel, the two decays can be adequately approximated with single exponentials, yielding values of ~0.35 ns for the polymer-QW and ~0.29 ns for the polymer-GaN structure. The ~21% increase in the fluorescence lifetime of the former indicates that a great

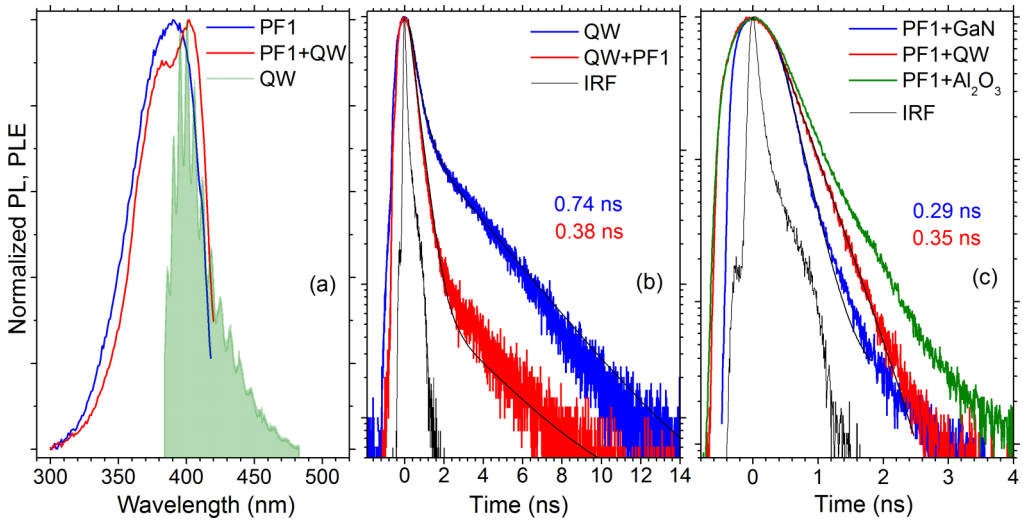

FIG. 6. (a) Room temperature normalized PLE of 10 nm PF1 films on sapphire (blue) and on a surface (Ga,In)N/GaN SQW (red) detecting at the 0-0 vibronic of PF1. The 300 K QW PL spectrum excited at 350 nm is also displayed in green. (b) Time-resolved PL decays of the SQW, monitoring the QW peak within a 10 nm spectral window, in the absence (blue) and presence (red) of the PF1 overlayer. The instrument response function (IRF) is also shown. Bi-exponential fits of the decays are displayed in black. (c) Time-resolved PL decays of the 0-0 vibronic PF1 fluorescence from films deposited on the SQW wafer (red) and reference PF1 films on GaN (blue) and Al_2O_3 (green). Single exponential fits are displaying in black.

fraction of the energy out-flown from the QW is resonantly transfered into the polymer excitations; to directly calculate the energy transfer yield, a more sophisticated modelling of the hybrid interaction is required.

C. FRET competing mechanisms

Samples with behavior not consistent with the spectra of Figure 6 allow us to identify loss mechanisms in the energy transfer process and correlate them with structural parameters of the hybrid structures. A first such mechanism can be observed in Figure 6(c); the PL decays obtained from the two films on the nitride wafers appear shortened compared to transients from identical films deposited on sapphire (Al_2O_3) substrates. The origin of the PL quenching of PF1 films on GaN has been studied elsewhere[41] and predominantly attributed to photoinduced electron transfer process from the polyfluore to GaN, providing an additional recombination channel for the PF1 photoexcitations. Back-transfer of carriers in the inorganic component or quenching of the transfer excitations at the heterointerface appears as a generic loss factor for FRET across inorganic/organic hybrids that tend to exhibit a type-II band alignment owing to the large electron affinity of the inorganic compared to the organic component; i.e., the effect has been also observed in FRET-coupled ZnO/oligomer structures.[9] A recent publication demonstrated an elegant scheme of cascade energy transfer to a second acceptor material, circumventing the loss by funneling the energy away from the interface.[45]

A second loss mechanism has been predominantly observed in hybrid structures employing (Al,Ga)N top caps. Figures 7(a) and 7(b) contain the transient PL data from the (Ga,In)N well with a 4 nm (Al,Ga)N cap with a 0.1 AlN mole fraction, in the presence and absence of the PF1 overlayer. A shortening of the QW PL lifetime of ~29% at room temperature and ~65% at 77 K is observed in the hybrid structure. However, the quenching of the energy donor lifetime is not accompanied by a concomitant lengthening of the rise time or the lifetime of PF1 that would signature the energy channeling process to the organic. Instead, the PF1/QW fluorescence decay appears similar or slightly faster than the decay of an identical film on GaN as observed in Figure 7(c). The time-resolved data are supported by comparative steady-state PL spectra that yield, in general, higher integrated areas from films deposited at GaN compared to identical films on the (Ga,In)N/(Al,Ga)N wafers. Such experiments have been performed with an excitation of 375 nm, i.e., below the GaN band-edge so the PL difference cannot be attributed to radiative pumping of the films by GaN. The aforementioned experiments indicate an efficient depletion of the QW excitations in the presence of the organic layer; however, the energy appears not to be transferred into the PF1 electronic states but it is dissipated elsewhere, most probably at the hybrid interface. Processes that transfer energy to surface states and compete with the FRET interaction, reducing its overall efficient, have been demonstrated recently in GaN/nanocrystal hybrids.[42] The higher contribution of such effects in hybrids based on (Al,Ga)N compared to GaN surfaces may be related to the significant higher oxidation of the former. Polyfluorene films on such surfaces may influence the surface band bending promoting localization of holes at the surface as observed in the highly confined SQW structure of Figure 3. The barrier confined holes can then recombine efficiently at the interface. Alternatively, the nitride valence band-PF1 HOMO band offset of ~0.6 eV[41] can promote their transfer to the polymer states. Both of the two mechanisms result in quenching of luminescence without concomitant transfer of energy on the organic material. Insight into the exact nature of the loss mechanism requires a detailed characterization of the (Al,Ga)N/polyfluorene interface similar to the work produced for GaN/polyfluorene hybrid structures.[41]

D. Correlation of FRET with the quantum well PL efficiency

Figure 8(c) contains the summary of our FRET studies based on assemblies of the three QWs of Figure 5, with

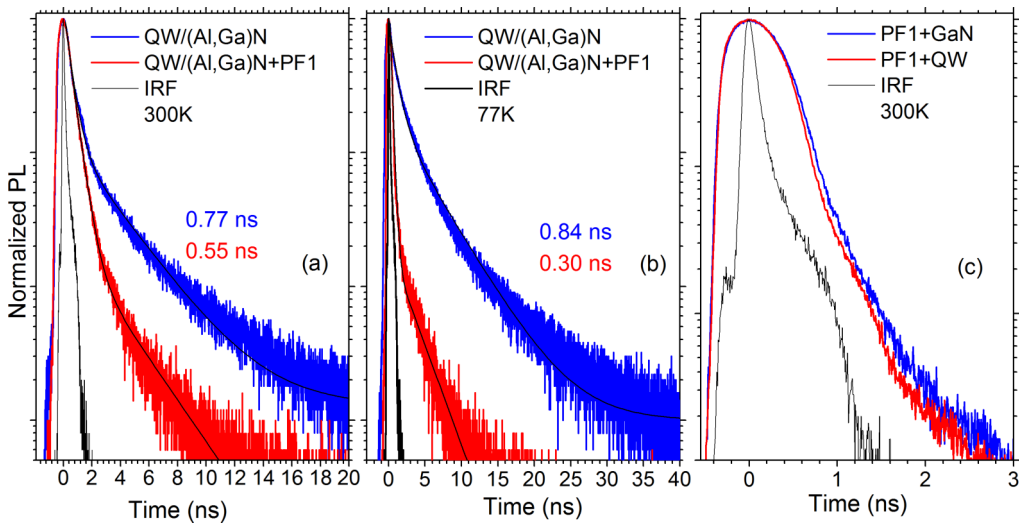

FIG. 7. (a) Room temperature time-resolved PL from a (Ga,In)N/(Al,Ga)N SQW in the absence (blue) and presence (red) of a 10 nm PF1 overlayer, detecting at the QW peak within a 10 nm bandwidth. (b) QW decays from the same samples at 77 K in the absence (blue) and presence (red) of the PF1 overlayer. (c) Time-resolved fluorescence of the 0-0 PF1 vibronic, within a 5 nm spectral window, from films deposited on the SQW wafer (red) and reference PF1 film on GaN (blue).

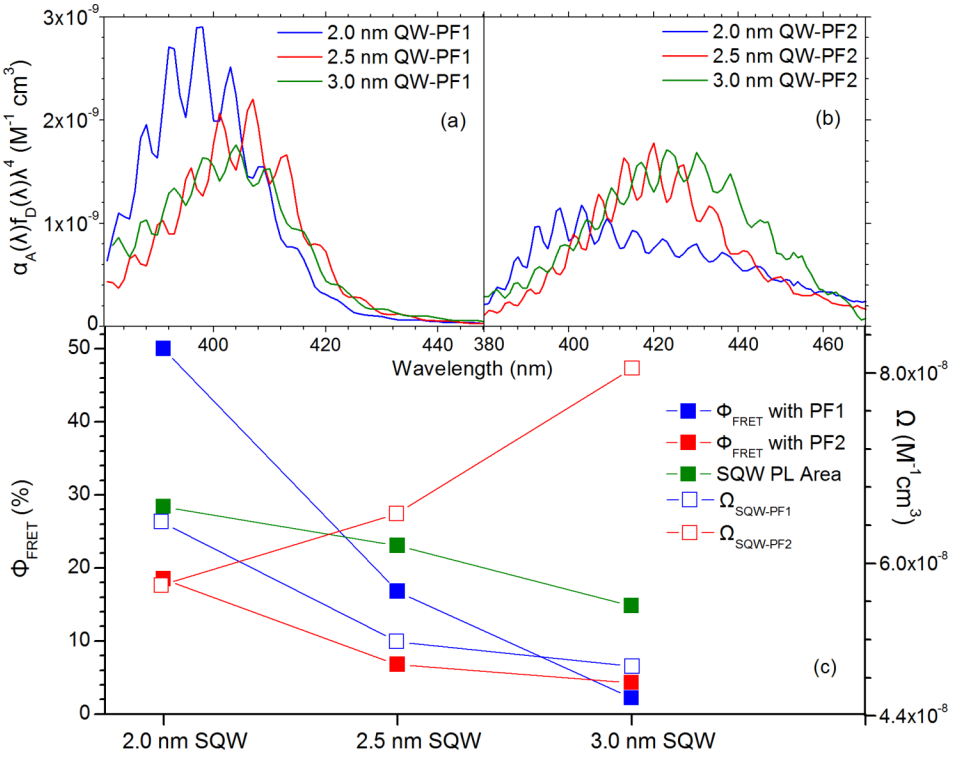

FIG. 8. (a) and (b) Products of the area-normalized emission of three SQWs with different well widths with the molar absorptivity $\alpha_A(\lambda)$ of PF1, PF2, respectively. (c) FRET efficiency (blue, red solid symbols), spectral overlap (Ω) (blue, red hollow symbols) and QW PL integrated area (green solid symbols) for hybrid structures based on PF1, PF2, and the three SQWs.

the homopolymer PF1 and the copolymer PF2. It can be observed that as the QW width increases from 2 to 3 nm, Φ_{FRET} reduces from 50% to 2.5% in PF1 hybrids (blue solid symbols) and from 18.5% to 4% in PF2 hybrids (red solid symbols). The general observation of higher FRET rates in the PF1 hybrids could be due to the observed preferential planar alignment of the homopolymer chains in thin films such as those employed in this study[41] that could enhance the dipole-dipole coupling. To interpret the behavior of Φ_{FRET} vs SQW width, we refer to Equation (1). QW width variation in the hybrid structures directly affects φ_D, τ_D (see Figure 3) and Ω. To examine the influence of the latter, Figures 8(a) and 8(b) display the wavelength scale products of the polymer (energy acceptor) molar absorptivity $\alpha_A(\lambda)$ with the area-normalized emission spectra of the 3 QWs (energy donor). The integral of such products yields the spectral overlap Ω.[2] The molar absorptivity of PF1, PF2 is computed in units of M^{-1} cm^{-3}, with M = mol m^{-3} using the following equation:[46]

$$a_A(\lambda) = \frac{A(\lambda)}{cl}, \tag{8}$$

where $A(\lambda)$ is the polymer film absorbance, c is the concentration in mol L^{-1} and l is the absorption path length approximated with the film thickness obtained from profilometry measurements; c is calculated using an average molecular weight of 100 000 for PF1 and 150 000 for PF2 based on the material supplier provided range.

The calculated spectral overlaps of the three QWs with PF1 (blue hollow symbols) and PF2 (red hollow symbols) are plotted in the graph of Figure 8(c) along with the respected FRET efficiencies and integrated QW PL area in the absence of organics, which can be considered as an approximate measure of φ_D. For hybrids based on PF1, the reduction of both spectral overlap and PL integrated area with QW width appears consistent with the reduction of Φ_{FRET} within the Förster model (Equation (1)). However for hybrids based on the PF2 polymer, proportionality is observed only between FRET efficiency and QW intensity. QW emission red-shifts as the QW width increases, increasing the spectral overlap with PF2 absorbance; however, the FRET rates reduce, exhibiting the opposite trend. Taking into account that the PL lifetime (Figure 5(b)) of the 2.0 and 2.5 nm SQWs is quite similar yet the two QW-based hybrids exhibit substantially different energy transfer rates to PF1 and PF2, we can conclude that out of the three factors, i.e., φ_D, τ_D, and Ω of Equation (1) that are influenced by the QW width, the first appears to have the dominant effect in the efficiency of the energy transfer process. The result validates our approach to optimize FRET by exploring the nitride structural parameters that affect the SQW luminescence in the absence of the organic acceptor.

E. Influence of electronic doping on FRET

The last part of our effort was focused on the investigation of electronic doping on the optical properties and FRET characteristics of the hybrid structures. The implementation of GaN doping appears as a prerequisite step for the realization of practical electrically excited FRET-based light emitting diodes (LEDs).[27] Conventional UV-emitting GaN LEDs rely on p-i-n structures; however, the requirement for an ultrathin top doped-layer to support the short-range FRET interaction dictates an n-i-p design as conductivities achievable in n-GaN are order of magnitude higher than those in p-type GaN.[16,27] An early demonstration of the aforementioned design using CdSe nanocrystals as energy acceptors produced a significantly high color-conversion efficiency of the order of 10%.[16] Proof-of-principle demonstration of FRET was demonstrated also on i-p[20] and p-i-n patterned GaN LEDs;[47]

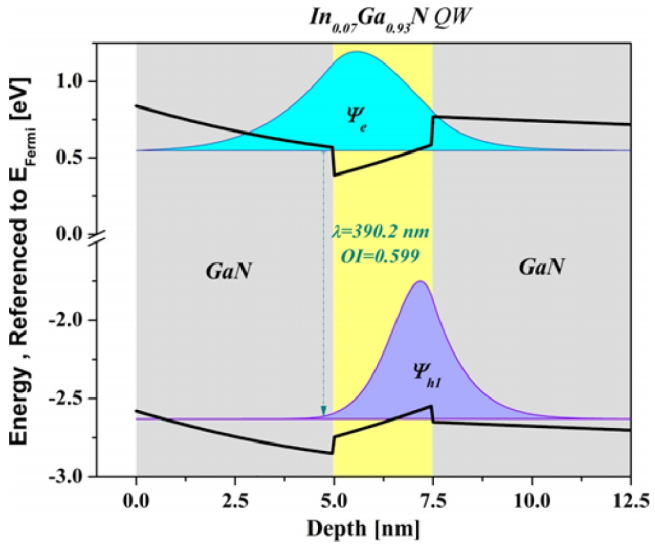

FIG. 9. SCSP-produced heterostructure profile and QW electron-hole eigenfunctions and eigenstates for a 2.5 nm SQW with InN mole fraction of 0.07 capped by a 5 nm GaN barrier, silicon doped at 5.0×10^{18} cm^{-3}.

however, to our knowledge, no studies where the influence of doping on FRET has been explicitly examined have been reported to date.

Focusing on the n-i-p design of Ref. 14, our study involved the investigation of nitride SQWs and hybrid structures employing an n(Si)-doped top GaN cap. The test structures retained the optimized characteristics of the undoped wafers with only varied parameter the n-doping level of the top cap, controlled by the Si dopant cell temperature and continuously tuned from non-intentional doped (NID), i.e., $\sim 1 \times 10^{16}$ cm^{-3} to n-doped at levels as high as 5×10^{18} cm^{-3}. The effects of doping were initially probed with our SCSP calculation model. In Figure 9, the heterostructure potential profile and the corresponding electron and hole eigenfunctions are shown, for a silicon doped (5.0×10^{18} cm^{-3}) 5 nm top GaN barrier. Top barrier doping appears to result in a deepening of the QW band levels with respect to the undoped case. As a result, the electron eigenfunction shifts closer to the InGaN QW, while the hole eigenfunction is only slightly affected, resulting overall in a significant increase of the electron-hole wavefunctions overlap. In the particular case treated, a significant increase of the transition oscillator strength by ~14% is estimated. Interestingly, the model indicates that doping produces an insignificant change in the difference of electron and hole eigenenergies and thus a negligible shift of the QW transition wavelength. Modelling thus predicts the beneficial role of n-doping of the top barrier that can lead to an increase of the SQW PL yield and correspondingly an increase of the FRET efficiency.

Despite the model prediction, our experimental studies indicate that for the majority of doped-wafers studied, doping has a detrimental effect on the PL efficiency. The trend is represented in Figure 10(a), for three SQWs produced in a single MBE run, where increase of the GaN n-doping results in efficient quenching of the low temperature (Ga,In)N well emission. Due to the quenching, a small subset of doped SQWs only exhibits room temperature PL. The PL quenching appears to be accompanied by a concomitant reduction of the FRET efficiency in hybrid structures with thin PFI ovelayers, as observed in Figure 10(b). For example, for the intermediate doped SQW of the figure, with a Si doping of $\sim 6 \times 10^{17}$ cm^{-3}, a SQW lifetime quenching of ~14% is measured at 77 K. Overall, measured PL quenching values in the presence of both PF1 and PF2 films are limited below 15%, setting this value as the higher bound of FRET efficiency in hybrids employing a doped-interlayer between the QW donor and the organic acceptor. The value is significantly lower than the respective high bounds of ~65% obtained for the undoped hybrid versions. It appears thus that in the simple doping scheme used, n-doping influences both the intrinsic properties of SQW and the characteristics of the hybrid interaction. It is quite possible that doping in such a close proximity to the emission layer leads to dopant diffusion into the well and collisional exciton recombination affecting the QW PL quantum yield. A reduction of the SQW emission yield would then strongly influence the FRET process, as demonstrated above.

In summary, we performed a systematic investigation of FRET within a hybrid prototype structure based on a nitride quantum well donor and a light emitting polymer acceptor. Initially, a combination of self-consistent Schrödinger-Poisson

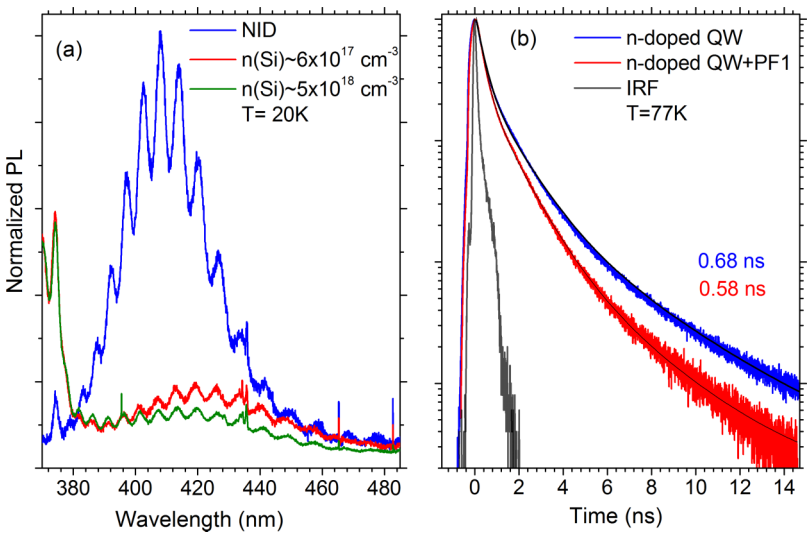

FIG. 10. (a) Comparative 20 K PL spectra of (Ga,In)N SQWs with top GaN cap doped at different Si-levels. The PL was non-resonantly excited at 350 nm. (b) QW decays at 77 K, monitoring the PL peak with a 10 nm bandwidth, from the n-doped SQW with Si $\sim 6 \times 10^{17}$ cm^{-3} in the absence (blue) and presence (red) of a PF1 overlayer.

modeling, MBE growth runs, and steady-state and time-resolved photoluminescence experiments were employed to investigate the influence of a wide structural parameter space of the nitride component that included growth temperature, material composition, and thickness of the well and barrier material. The energy transfer process was subsequent studied in hybrid structures completed with spin-casted overlayers of two polyfluorene materials. Unexplored aspects of the dipole-dipole coupling were probed and correlated to the characteristics of the nitride quantum well and the hybrid interface. Important conclusions of the study have been the beneficial effect of the quantum well confinement on the nitride PL emission and the experimental establishment of the strong correlation between the intrinsic photoluminescence yield of the nitride and the FRET efficiency in the completed hybrid structure. The methodology could potentially be applied to other hybrid planar combinations, providing an initial and relatively simple FRET optimization step based on luminescence studies of the inorganic donor structure in the absence of an energy acceptor.

The study has also demonstrated three significant loss mechanisms that compete with the FRET process: 1. Recombination of the SQW excitations at the interface or hole transfer to the organic material; the effect appears more intense in hybrids containing high Al content that appears to promote hole localization at the barrier, 2. back transfer of carriers and/or interfacial quenching subsequent to the transfer of energy in the organic acceptor, and 3. quenching of the SQW emission and FRET efficiency in the presence of an n-doped nitride interlayer. The loss mechanisms should not be in principle inherent to the specific hybrid pair of donor-acceptor materials and may pose as a general limitation of FRET efficiency in electrical-pumped devices based on the simple planar geometry studied. Design of the inorganic heterostructure to ensure strong confinement of carriers in the quantum well and adequate spatial separation from the interface may reduce losses associated with the mechanism. 1. In any case, a detailed investigation of the hybrid interface appears as a necessary step towards the understanding of interfacial recombination that competes with FRET in each hybrid pair. More elaborate schemes that efficiently funnel the transferred energy away from the interface[45] or appropriately tailor the hybrid band-offsets reducing the driving force for energy back-transfer[47] could circumvent the losses associated with the mechanism. 2. Losses associated with doping are most probably associated with the close proximity of the quantum well and doped region resulting in non-radiative quenching of the well excitons and a subsequent reduction of FRET. More sophisticated approaches such as the use of patterned nitride structures[48] that enable a larger separation between the doped barrier and the active well region could circumvent the problem; however, electronic doping appears as a potential limitation of FRET requiring further investigation on the mechanisms via which it affects the dipole-dipole interaction.

ACKNOWLEDGMENTS

G. Itskos, A. Othonos, S. Choulis, and E. Iliopoulos thank the Cyprus Research Promotion Foundation for financial support of the project via the infrastructure upgrade research Grant "No. ANABAΘMIΣH/0609/15."

[1]T. Förster, Discuss. Faraday Soc. **27**, 7 (1959).
[2]G. D. Scholes, Annu. Rev. Phys. Chem. **54**, 57 (2003).
[3]V. M. Agranovich, G. C. La Rocca, and F. Bassani, JETP Lett. **66**, 748 (1997).
[4]D. Basko, G. C. La Rocca, F. Bassani, and V. M. Agranovich, Eur. Phys. J. B **8**, 353 (1999).
[5]V. M. Agranovich, D. M. Basko, G. C. La Rocca, and F. Bassani, Synth. Met. **116**, 349 (2001).
[6]M. Achermann, M. A. Petruska, S. Kos, D. L. Smith, D. D. Koleske, and V. I. Klimov, Nature **429**, 642 (2004).
[7]G. Heliotis, G. Itskos, R. Murray, M. D. Dawson, I. M. Watson, and D. D. C. Bradley, Adv. Mater. **18**, 334 (2006).
[8]S. Blumstengel, S. Sadofev, C. Xu, J. Puls, and F. Henneberger, Phys. Rev. Lett. **97**, 237401 (2006).
[9]S. Blumstengel, S. Sadofev, and F. Henneberger, New J. Phys. **10**, 065010 (2008).
[10]A. A. R. Neves, A. Camposeo, R. Cingolani, and D. Pisignano, Adv. Funct. Mater. **18**, 751 (2008).
[11]Q. Zhang, T. Atay, J. R. Tischler, M. S. Bradley, V. Bulovic, and A. V. Nurmikko, Nat. Nanotechnol. **2**, 555 (2007).
[12]S. Chanyawadee, P. G. Lagoudakis, R. T. Harley, D. G. Lidzey, and M. Henini, Phys. Rev. B **77**, 193402 (2008).
[13]G. W. Shu, C. C. Lin, H. T. Lin, T. N. Lin, J. L. Shen, C. H. Chiu, Z. Y. Li, H. C. Kuo, C. C. Lin, S. C. Wang, C. A. J. Lin, and W. H. Chang, Opt. Express **19**, A194 (2011).
[14]Z. Chen, S. Berciaud, C. Nuckolls, T. F. Heinz, and L. E. Brus, ACS Nano **4**, 2964 (2010).
[15]F. Federspiel, G. Froehlicher, M. Nasilowski, S. Pedetti, A. Mahmood, B. Doudin, S. Park, J.-O. Lee, D. Halley, B. Dubertret, P. Gilliot, and S. Berciaud, Nano Lett. **15**, 1252 (2015).
[16]M. Achermann, M. A. Petruska, D. D. Koleske, M. H. Crawford, and V. I. Klimov, Nano Lett. **6**, 1396 (2006).
[17]C. R. Belton, G. Itskos, G. Heliotis, P. N. Stavrinou, P. G. Lagoudakis, J. Lupton, S. Pereira, E. Gu, C. Griffin, B. Guilhabert, I. M. Watson, A. R. Mackintosh, R. A. Pethrick, J. Feldmann, R. Murray, M. D. Dawson, and D. D. C. Bradley, J. Phys. D: Appl. Phys. **41**, 094006 (2008).
[18]G. Itskos, C. R. Belton, G. Heliotis, I. M. Watson, M. D. Dawson, R. Murray, and D. D. C. Bradley, Nanotechnology **20**, 275207 (2009).
[19]S. Nizamoglu, E. Sari, J.-H. Baek, I.-H. Lee, and H. V. Demir, New J. Phys. **10**, 123001 (2008).
[20]S. Nizamoglu, E. Sari, I.-H. Lee, J.-H. Baek, and H. V. Demir, IEEE J. Sel. Top. Quantum Electron. **15**, 1163 (2009).
[21]D. L. Dexter, J. Lumin. **18-19**, 779 (1979).
[22]D. M. Basko, G. L. La Rocca, F. Bassani, and V. M. Agranovich, Phys. Rev. B **71**, 165330 (2005).
[23]V. M. Agranovich, V. I. Rupasov, and L. Silvestri, Phys. Status Solidi C **7**, 1684 (2010).
[24]S. Chanyawadee, R. T. Harley, M. Henini, D. V. Talapin, and P. G. Lagoudakis, Phys. Rev. Lett. **102**, 077402 (2009).
[25]S. Nizamoglu, B. Guzelturk, D.-W. Jeon, I.-H. Lee, and H. V. Demir, Appl. Phys. Lett. **98**, 163108 (2011).
[26]R. Smith, B. Liu, J. Bai, and T. Wang, Nano Lett. **13**, 3042 (2013).
[27]V. M. Agranovich, Y. N. Gartstein, and M. Litinskaya, Chem. Rev. **111**, 5179 (2011).
[28]P. L. Hernández-Martínez, A. O. Govorov, and H. V. Demir, J. Phys. Chem. C **117**, 10203 (2013).
[29]G. Itskos, G. Heliotis, P. G. Lagoudakis, J. Lupton, N. P. Barradas, E. Alves, S. Pereira, I. M. Watson, M. D. Dawson, J. Feldmann, R. Murray, and D. D. C. Bradley, Phys. Rev. B **76**, 035344 (2007).
[30]Y. Gladush, C. Piermarocchi, and V. Agranovich, Phys. Rev. B **84**, 205312 (2011).
[31]Š. Kos, M. Achermann, V. I. Klimov, and D. L. Smith, Phys. Rev. B **71**, 205309 (2005).
[32]S. Rohrmoser, J. Baldauf, R. T. Harley, P. G. Lagoudakis, S. Sapra, A. Eychmuller, and I. M. Watson, Appl. Phys. Lett. **91**, 092126 (2007).
[33]J. J. Rindermann, G. Pozina, B. Monemar, L. Hultman, H. Amano, and P. G. Lagoudakis, Phys. Rev. Lett. **107**, 236805 (2011).
[34]S. Kawka and G. C. La Rocca, Phys. Rev. B **85**, 115305 (2012).
[35]G. Heliotis, E. Gu, C. Griffin, C. W. Jeon, P. N. Stavrinou, M. D. Dawson, and D. D. C. Bradley, J. Opt. A **8**, S445 (2006).

[36]M. Wu, Z. Gong, A. J. C. Kuehne, A. L. Kanibolotsky, Y. J. Chen, I. F. Perepichka, A. R. Mackintosh, E. Gu1, P. J. Skabara, R. A. Pethrick, and M. D. Dawson, Opt. Express **17**, 16436 (2009).
[37]M. Boroditsky, I. Gontijo, M. Jackson, R. Vrijen, E. Yablonovitch, T. Krauss, C. C. Cheng, A. Scherer, R. Bhat, and M. Krames, J. Appl. Phys. **87**, 3497 (2000).
[38]A. Othonos, G. Itskos, D. D. C. Bradley, M. D. Dawson, and I. M. Watson, Appl. Phys. Lett. **94**, 203102 (2009).
[39]O. Kopylov, R. Shirazi, O. Svensk, S. Suihkonen, S. Sintonen, M. Sopanen, and B. E. Kardynał, Phys. Status Solidi C **9**, 727 (2012).
[40]O. Svensk, S. Suihkonen, S. Sintonen, O. Kopylov, R. Shirazi, H. Lipsanen, M. Sopanen, and B. E. Kardynal, Phys. Status Solidi C **9**, 1667 (2012).
[41]G. Itskos, X. Xristodoulou, E. Iliopoulos, S. Ladas, S. Kennou, M. Neophytou, and S. Choulis, Appl. Phys. Lett. **102**, 063303 (2013).
[42]O. Kopylov, A. Huck, S. Kadkhodazadeh, K. Yvind, and B. Kardynal, J. Phys. Chem. C **118**, 16284 (2014).
[43]O. Ambacher, J. Majewski, C. Miskys, A. Link, M. Hermann, M. Eickhoff, M. Stutzmann, F. Bernardini, V. Fiorentini, V. Tilak, B. Schaff, and L. F. Eastman, J. Phys.: Condens. Matter **14**, 3399 (2002).
[44]S. Adachi, *Optical Constants of Crystalline and Amorphous Semiconductors: Numerical Data and Graphical Information* (Springer Science and Business Media, NY, 1999).
[45]F. Bianchi, S. Sadofev, R. Schlesinger, B. Kobin, S. Hecht, N. Koch, F. Henneberger, and S. Blumstengel, Appl. Phys. Lett. **105**, 233301 (2014).
[46]IUPAC, in *Compendium of Chemical Terminology (The "Gold Book")*, 2nd ed., compiled by A. D. McNaught A. Wilkinson (Blackwell Scientific Publications, Oxford, UK, 1997).
[47]S. Chanyawadee, P. G. Lagoudakis, R. T. Harley, M. D. B. Charlton, D. V. Talapin, H. W. Huang, and C.-H. Lin, Adv. Mater. **22**, 602 (2010).
[48]R. Schlesinger, F. Bianchi, S. Blumstengel, C. Christodoulou, R. Ovsyannikov, B. Kobin, K. Moudgil, S. Barlow, S. Hecht, S. R. Marder, F. Henneberger, and N. Koch, Nat. Commun. **6**, 6754 (2015).